Applied Catalysis B: Environmental 328 (2023) 122459

Contents lists available at ScienceDirect

Applied Catalysis B: Environmental

journal homepage: www.elsevier.com/locate/apcatb

Efficient full dechlorination of chlorinated ethenes on single enzyme-like Co−N_4 sites in nitrogen-doped carbons

Hejie Qin [a,b], Tanjie Zha [b], Kun Qian [c], Yuankui Sun [a], Xiaohong Guan [a,b,*], Chuncheng Chen [d,**]

[a] Shanghai Engineering Research Center of Biotransformation of Organic Solid Waste, School of Ecological and Environmental Sciences, East China Normal University, Shanghai 200241, PR China
[b] State Key Laboratory of Pollution Control and Resources Reuse, College of Environmental Science and Engineering, Tongji University, Shanghai 200092, PR China
[c] Department of Environmental Science, School of Environmental Science and Engineering, Suzhou University of Science and Technology, Suzhou 215009, PR China
[d] Key Laboratory of Photochemistry, CAS Research/Education Center for Excellence in Molecular Sciences, Institute of Chemistry, Chinese Academy of Sciences, Beijing 100049, PR China

ARTICLE INFO

Keywords:
Reductive dechlorination
Trichloroethene
Dehalogenase
Single-atom catalyst
Enzyme mimics

ABSTRACT

Chlorinated ethenes are ubiquitous contaminants in groundwater. Here, by embedment of enzyme-like Co−N_4 sites in the nitrogen-doped carbon support, we prepared a Co−NC catalyst to combine the advantages of abiotic and biological dechlorination strategies. Co−NC exhibited superior reactivity and stability for catalytic dechlorination of chlorinated ethenes under various conditions. Up to 94.8% of trichloroethene could be transformed directly to acetylene without toxic intermediates. Moreover, Co−NC could utilize electrons from dissolved Fe(II), which is low-cost and a common component in the groundwater, making the Co−NC-based strategies sustainable for the remediation. Even with such a weak reductant, acetylene was still the dominant product. Those catalytic properties originate from the synergism of the nitrogen-doped carbons and the highly active Co sites. This synergism favors a mechanism where the toxic intermediates are bound on Co sites until the full dechlorination, due to the excellent electron-storage ability and the electronic delocalization characteristic of nitrogen-doped carbons.

1. Introduction

Chlorinated ethenes rank among the most predominant pollutants in groundwater [1], due to their widespread use, improper disposal, and substantial emission to the environment [2]. Their environmental risks largely originate from the chlorine substituents, and as the number of chlorine substituents increases, the tendency for oxidative degradation decreases [3], because of the strong electron-withdrawing effects of these substituents. Therefore, continuous efforts have been focused on reductive dechlorination strategies as the solution to their contamination [4], since the non-chlorinated products are non-toxic to the environment or more easily degraded. Several abiotic and biological remediation strategies have been developed for the dechlorination of chlorinated ethenes. The abiotic ones include direct reduction [5,6], Pd-based catalysis [7], electrocatalysis [8], photocatalysis processes [9], etc. The biological strategy mainly refers to bioremediation using organohalide-respiring bacteria (ORB), which are an integral part of subsurface ecosystems [10].

Among them, the bioremediation approaches offer some advantages over the abiotic ones, based on their viability under mild and easily scalable conditions [11], which may make them more environmentally sustainable [12]. To begin with, they show excellent biocompatibility and pose fewer secondary impacts on ecosystems, because they do not rely on strong and excessive reductants. These reductants are generally required in direct reduction strategies, due to the low redox potential of chlorinated ethenes (e.g., E_h^1 of trichloroethylene (TCE) is ca. − 0.7 V vs SHE [13]). In contrast, a broader range of electron donors can be utilized in a biochemical process, including the weaker while environmentally benign ones [14]. For the same reason, they do not suffer from some intrinsic drawbacks of commonly used conventional reductants, e.g., zerovalent iron, including passivation and low mobility of the (nano) particles [15,16]. Meanwhile, bio-dechlorination processes may have

* Corresponding author at: Shanghai Engineering Research Center of Biotransformation of Organic Solid Waste, School of Ecological and Environmental Sciences, East China Normal University, Shanghai 200241, PR China.
** Corresponding author.
E-mail addresses: xhguan@des.ecnu.edu.cn (X. Guan), ccchen@iccas.ac.cn (C. Chen).

https://doi.org/10.1016/j.apcatb.2023.122459
Received 15 December 2022; Received in revised form 7 February 2023; Accepted 9 February 2023
Available online 11 February 2023

greater potential for scale-up compared with current abiotic catalysis, although both of them exhibit good performance in bench-scale studies [8,9,17]. From a remediation standpoint, the required electric fields, photo fields, and hydrogen gas are technically hard to be supplied in a large-scale groundwater system, not to mention their exorbitant costs and/or high energy input.

All of those advantages of bio-dechlorination processes lie on the high activity of ORB, or more specifically, their membrane-associated enzyme, reductive dehalogenase (RDase) [18,19]. The typical class of RDases is cobalamin (vitamin B_{12}, VB_{12})-dependent enzymes, i.e., each of them harbors a VB_{12} cofactor as the catalytic subunit. The native role of VB_{12}-dependent RDase in the global chlorine cycle, as well as their possible application in organohalide respiration, has motivated intensive research on their molecular structure and VB_{12}-mediated chemistry [20,21]. VB_{12} contains a Co atom coordinated to 4 ring N atoms (Co−N_4). With the electron transferred to the Co atom, it can be reduced to nucleophilic Co(I) with high activity. Co(I) can directly attack on carbon bearing the chlorine substituent, resulting in the cleavage of a C−Cl bond and the subsequent elimination of the chlorine atoms. Then this dechlorinated intermediate is protonated, resulting in the formation of hydrogenolysis products [20,22]. A typical example is that TCE is sequentially dechlorinated to *cis*-dichloroethene (*cis*-DCE), vinyl chloride, and ethene during the RDase-catalyzed reduction.

Notwithstanding lots of advantages, significant challenges still remain to be addressed for the application of bio-dechlorination processes. The major ones are the generation of a sufficient quantity of ORB or RDases with desired ability, and their low physiochemical tolerances against environmental conditions. Those could lead to the absence of dechlorination activity, or even worse, the accumulation of intermediates, such as *cis*-dichloroethene (*cis*-DCE) and vinyl chloride [23], which are less reactive but more problematic than their parent compounds [24]. Those limitations call for further exploration, and one promising countermeasure is to replace the natural enzymes with synthesized mimics. The feasibility of this solution has been positively assessed in recent studies on avoiding the intrinsic drawbacks of natural enzymes in various biological applications [25]. Therefore, a synthesized catalyst with RDase-like activity, a facile production method, and high stability is desired. Dechlorination processes with that catalyst could combine the advantages of biological and chemical catalysis and lead to an ideal dechlorination strategy.

The carbon-supported single-atomic transitional metal catalysts could be an attractive platform to satisfy the demands, which have been showing great potential in heterogeneous catalysis [26–28]. Their utmost atom utilization and unique coordination environments of metal sites endowed them with the activity for some metalloenzyme-catalyzed reactions [29–31]. Single-atomic Co sites embedded in a carbon support may be feasible for mimicking the dechlorination reactivity of RDases because of the same metal center. More importantly, the microenvironment and consequently the catalytic properties of metal sites could be readily modulated by doping the carbon support using heteroatoms such as N and B [32,33]. As one of the natural components of RDases, N could form moieties that influence the reaction pathways and thereby change the dechlorination products by affecting the outer-sphere environment of the Co−N_4 site [34,35]. That provides an opportunity to tune the catalytic properties of the reactive sites for optimal catalytic performance and desirable products.

Here, inspired by the active sites of VB_{12}-dependent RDases, we prepared a catalyst, which is characterized by the enzyme-like Co−N_4 sites embedded in the nitrogen-doped carbon support (Co−NC), to construct a new catalytic system. Its performance for dechlorination of chlorinated ethenes and various aspects were evaluated, including product distribution as well as the reactivity and stability of Co−NC. To compare with the catalytic activity and mechanism of the biocatalyst, Ti (III) served as the electron donor, because it is strong enough to give meaningful reaction rates in the biocatalyst systems and is most commonly used in the studies on RDases [20,36]. We also showed the possibility of utilizing dissolved Fe(II) as the electron donor, which is weak while cost-efficient and inherently co-existing in groundwater. The dechlorination mechanism based on the catalytic activity of Co−N_4 sites and the support effects of nitrogen-doped carbon support was proposed. We present a new application of the biomimetic catalyst in a catalytic dechlorination system without electric fields, photo fields, etc. Compared with the previous study on electrocatalysis [33], the way to supply electrons requires addressing extra technical and mechanistic issues to make sure effective interactions of catalysts with electron donors. This way to supply electrons, along with the catalytic activity under mild conditions makes the present system more suitable for groundwater remediation. Therefore, it could lead to a sustainable dechlorination strategy due to the energy-efficient and scalable ways to supply electrons, which also has practical implications for the field scale application.

2. Materials and methods

2.1. Materials

Details regarding the materials used are given in the Supplementary Material online.

2.2. Materials synthesis

In brief, a certain amount of Co(II)-phenanthroline complexes, 0.9 g glucose, and 0.6 g C_3N_4 were mixed in a solution. The mole ratio of $CoSO_4$ to 1,10-phenanthroline is 1:3 and a typical dosage of Co is 0.133 mmol, giving a final Co content of 1.8 wt% in the synthesized material. The mixture was freeze-dried and ground to obtain the precursor. The precursor was heated in a tube furnace at the rate of 5 °C/min to 800 °C under a gas flow of 0.2 L/min N_2 and pyrolyzed at this temperature for 2 h. The resulting product was ground to obtain Co−NC. Nitrogen-doped carbon without Co (NC) was prepared by the same procedure but without $CoSO_4$ and 1,10-phenanthroline. The synthesis procedure is demonstrated in Fig. S1 in the Supplementary Material.

2.3. Experimental procedures for TCE dechlorination

All experiments were performed in anaerobic and well-sealed batch reactors. All solutions were prepared using water or organic solutions that were degassed and stored in anaerobic chamber, unless otherwise specified. A certain amount of TCE stock solution (0.1 M in methanol) was injected into a 60-mL reactor containing Co−NC and 40 mL water. The pH was maintained by 50 mM MES (for pH 5.0 and 6.0), HEPES (for pH 7.0 and 8.0), and Tris (for pH 9.0). Then, the reactor was moved into a dark incubator and placed on a rotator (25 rpm, with the plane oriented 60° from horizontal) in it for 1 h at 25 °C, to achieved the adsorption−desorption equilibrium of TCE on the catalyst. It should be noted that TCE showed little loss from the reactor and little adsorption on the catalyst (Fig. S2). The stock solution of Ti(III)-citrate (0.5 M Ti (III)) was prepared by Ti(III) sulfate, trisodium citrate, and water (Ti (III):citrate = 1:2 (mole ratio)). Certain amount of 0.5 M Ti(III)-citrate and 6 M NaOH was injected to the reactor after the one-hour equilibrium. The typical doses of Ti(III)-citrate and NaOH were 0.6 mL and 0.125 mL, giving a final concentration of 7.4 mM Ti(III). For the kinetics of TCE reduction, the time 0 min corresponds to the time point of Ti(III) injection. At gradually increasing time intervals, the headspace sample (40 μL) was withdrawn for the detection of TCE and its daughter products by a gas chromatograph/mass spectrometer (GC/MS). Withdrawing the headspace sample would result in little dilution since the volume was neglectable. Another headspace sample (10 μL) of a 0.8 mM hexane solution was injected into the GC/MS right after the injection of TCE samples as an internal standard to correct for the mass loss during the sample inlet. For liquid sample, 0.4 mL N_2 was injected into the bottle, a 0.4 mL liquid sample was withdrawn, and the sample was

immediately filtered through a 0.22-μm membrane filter into a vial. The filtered sample was then acidified with 5 μL HNO_3 to preserve it until analysis. Experiments on PCE, with VB_{12}, or with Fe(II) followed the same procedures described above. In addition, because of the deficit of mass balance, thermal desorption was conducted. After reaction for 90 min, H_2SO_4 solution was injected into the reactor to adjust the pH to below 4.0, at which the further reaction was completely inhibited. Then the reactor containing Co was put into a water bath (90 °C) for 30 min. Headspace samples were withdrawn with the above-mentioned procedures when the reactor cooled down to the room temperature.

2.4. Computational methodology

The density functional calculations were performed by a method reported by Ji et al. [37] Briefly, the geometry optimizations were carried out by using PBE functional [38,39] and at the basis sets of Ahlrich's TZV [40] for Co and 6–31 G** [41] for C, N, H, O, and Cl. All DFT calculations were performed using the Gaussian 09 program package [42]. The orbital distribution was analyzed by Multiwfn code [43].

Other experimental details are elaborated in the Supplementary Material, including more detailed protocol for Co−NC synthesis, procedure of kinetic experiments, characterization of Co−NC, analysis of gas and liquid samples, and electrochemical measurements.

3. Results and discussion

3.1. Characterization of the Co−NC catalysts

A series of Co−NC catalysts was prepared by heat treatment of a

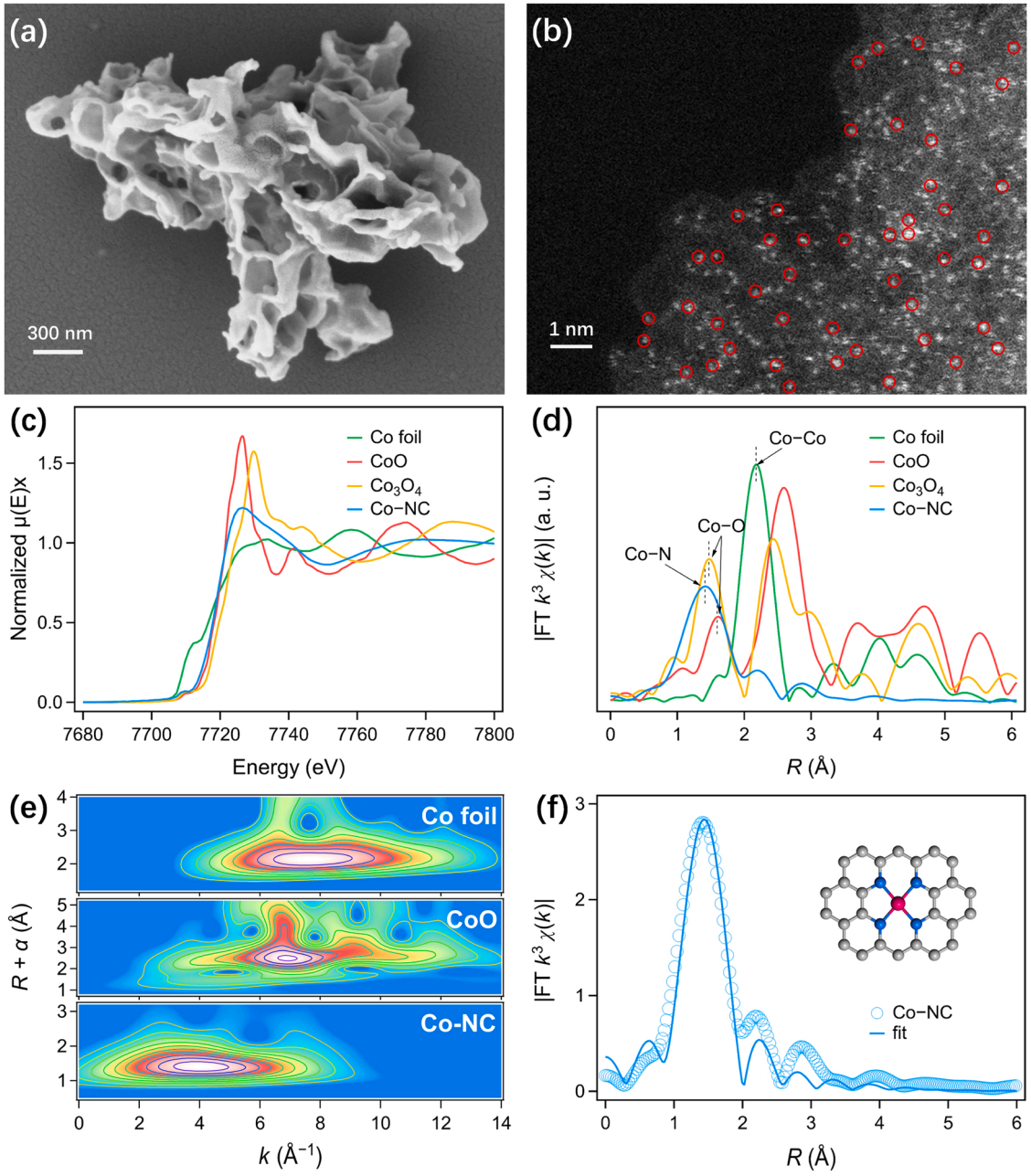

Fig. 1. (a) SEM and (b) HAADF-STEM images of Co−NC. (c) XANES and (d) Fourier-transformed (FT) k^3-weighted EXAFS spectra at the Co *K*-edge of Co−NC and reference samples including Co foil, CoO and Co_3O_4. (e) Wavelet transform (WT) of the EXAFS spectra of Co foil, CoO, and Co−NC. (f) EXAFS fitting curve of Co−NC at *R* space. Inset: atomic structure model of Co−NC, Co (purple), N (blue), and C (gray).

mixture of glucose, C_3N_4, and Co(II)-phenanthroline complexes under the protection of N_2 [44]. The glucose and Co(II)-phenanthroline complex served as the precursor of the carbon support and Co−N_4 moieties, respectively. The Co contents in the prepared Co−NC were found to be in the range of 0.6–3.1 wt% with inductively coupled plasma-optical emission spectrometry (ICP-OES). The Co−NC with 1.8 wt% Co was employed as the representative of this series of catalysts for further solid-phase characterization. Scanning electron microscopy (SEM) images showed that Co−NC has a highly porous sheet-like structure (Fig. 1**a**). Energy-dispersive X-ray spectroscopy (EDS, Fig. S3) images and X-ray photoelectron spectroscopy (XPS, Fig. S4a) analysis confirmed the presence of C, N, and Co in Co−NC. XPS analysis revealed the atom ratio of N in Co−NC was ~15.2 atom %. The Co content was ~0.44 atom % (2.0 wt%), consistent with the ICP-OES result (1.8 wt%) [34,45,46].

From the high-angle annular dark-field scanning transmission electron microscopy (HAADF-STEM, Fig. 1**b**) image, high-density bright dots, which are corresponding to the randomly dispersed single Co atoms, were observed, as highlighted by red circles in Fig. 1**b**. To further investigate the chemical state and coordination environment of Co species at the atomic level, X-ray absorption near-edge structure (XANES) and extended X-ray absorption fine structure (EXAFS) spectra at Co *K*-edge were collected. The XANES absorption edge position of Co−NC suggests that the oxidation state of Co is about + 2 (Fig. 1**c**), which is in accordance with the XPS result (Fig. S4c). The Fourier transform of the k^3-weighted EXAFS spectrum for Co−NC reveals that the first coordination shell of the Co element was located at ~1.4 Å, which is attributed to the Co−N coordination shell [47]. Notably, there is only one dominant peak, but no other high-shell peaks such as Co−Co (at ~2.2 Å) and Co−O coordination (at 1.5–1.6 Å) were observed (Fig. 1**d**). Such a spectral profile indicates that Co species are atomically dispersed in the Co−NC sample. To distinguish the backscattering atoms more clearly, the wavelet transform (WT) analysis was performed (Fig. 1**e**). Co−NC shows one WT maximum at ~4 $Å^{-1}$, which can be assigned to Co−N coordination, and no WT maximum corresponding to Co−Co or Co−O is detected. The quantitative coordination configuration of Co atoms in Co−NC can be determined with EXAFS fitting (Fig. 1**f**). The results demonstrate that the Co−N coordination number is about 4 and the average bond length is 2.02 Å (Table S1). Combining results from the above-mentioned characterizations of Co−NC, Co atoms are coordinated to 4 N atoms to form Co−N_4 centers embedded in the nitrogen-doped carbon support. It is also noted that although only the characterization results on Co−NC with 1.8 wt% Co are shown in detail, those on Co−NC with higher Co contents (3.1 wt%) were also performed and gave similar results.

3.2. *Catalytic performance for TCE dechlorination*

Kinetics. The activity of Co−NC catalysts was first tested by the reductive dechlorination of TCE, which is the most typical chlorinated contaminant in groundwater. As shown in Fig. 2**a**, with Ti(III)-citrate as the electron donor, dechlorination of TCE catalyzed by Co−NC (1.8 wt% Co) was efficient and nearly completed within 75 min. This rate was comparable to those in advanced reduction and electrocatalysis systems [9,48], which were considered as relatively fast abiotic dechlorination processes in previous studies. The results of blank and control experiments showed that TCE decay was neglectable in the absence of Co−NC and/or Ti(III)-citrate, indicating that both Co−NC and Ti(III)-citrate are indispensable for TCE reduction (Fig. S2). The nitrogen-doped carbon material without Co (NC) exhibited little catalytic activity for TCE dechlorination. With increasing Co contents in Co−NC, its catalytic

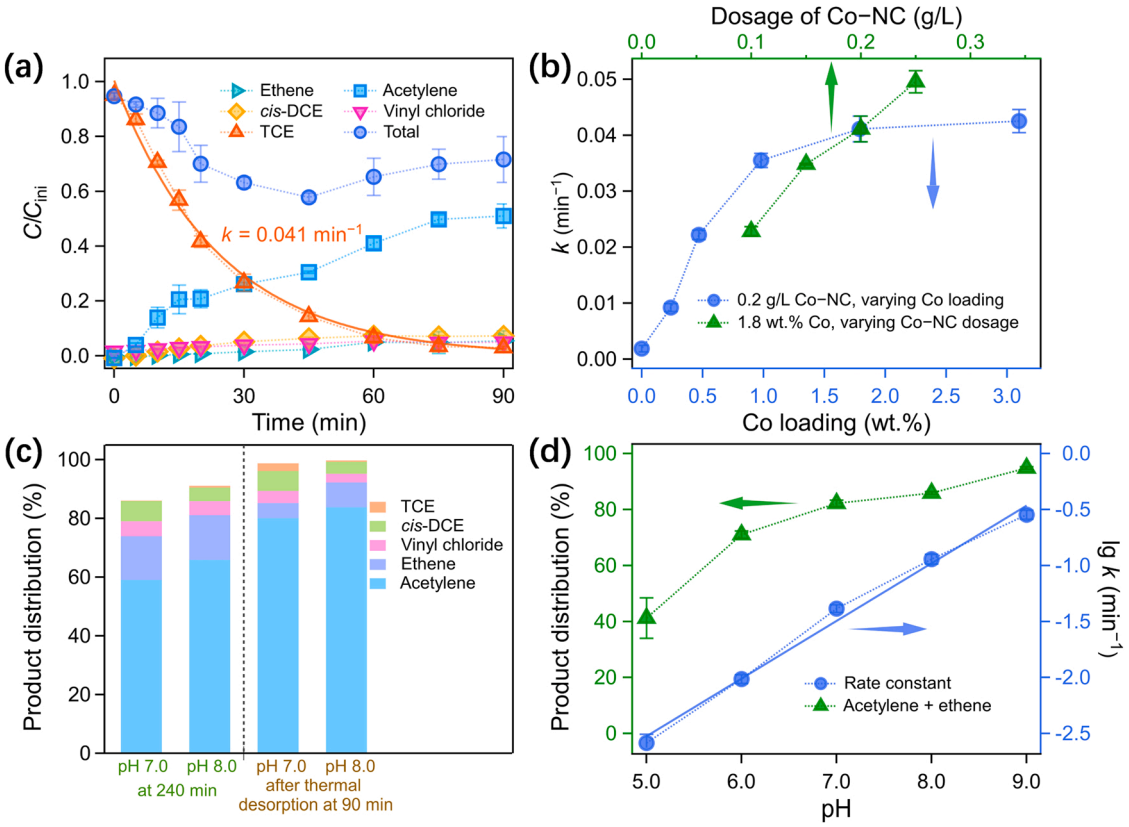

Fig. 2. (a) Kinetics of TCE dechlorination catalyzed by Co−NC (1.8 wt% Co) and the generation of its products at pH 7.0. Solid lines are the first-order fits. Reaction conditions: $[TCE]_0$ = 0.1 mM, [Co−NC] = 0.2 g/L, $[Ti(III)]_0$ = 7.4 mM, pH was maintained at 7.0 with 50 mM HEPES buffer, T = 25 °C, anaerobic condition. (b) The product distribution at 240 min and after thermal desorption at 90 min (c) Influence of pH on the first-order rate constants and the product distribution of TCE transformation. (d) First-order rate constants for TCE dechlorination at various Co loadings with 0.2 g/L Co−NC (blue markers), or various dosages of Co−NC with 1.8 wt% Co (green markers), respectively. The reaction conditions of (c-d) are the similar to those for Fig. 2a, except for the pHs and dosages denoted in the figures.

performance showed a tendency of increasing at the low content of Co, and leveled off when the Co loading was larger than 1.8 wt% (Fig. 2**b** and **S5**). These results indicate that Co sites are essential to the activity of the Co−NC catalyst. Also, if there are Co clusters formed at a concentration below the detection limit of the solid-phase characterization above, which does not support their formation, those clusters may not affect the dechlorination, because catalytic performance is similar at the Co loading of 1.8 wt% to that at 3.1 wt% and clusters are much more easily to form at a higher loading level. Moreover, that activity is nearly proportional to its dosage (Fig. S6 and green markers in Fig. 2**b**) and the concentration of the electron donor, Ti(III)-citrate (Fig. S7).

Product distribution. The most notable characteristic of the TCE dechlorination catalyzed by Co−NC is that acetylene was the dominant product. At pH 7.0, acetylene accounts for 74.3% of all the detected products at 90 min (Fig. 2**a**), accompanied by the release of Cl^- (Fig. S8). Only a minor amount of chlorinated products, *cis*-DCE (10.6%) and vinyl chloride (7.2%), were detected. Besides, a certain amount of ethene (8.0%) was also observed. With prolonged reaction time, the yield of ethene increased slowly (17.4% at 240 min), accompanied by the decrease of acetylene (Fig. 2**c**). This result indicates that the formation of ethene should be attributed to the further reduction of the formed acetylene under the present conditions, rather than to the hydrodechlorination of TCE. In addition, the acetylene should not originate from the secondary reaction of formed *cis*-DCE and vinyl chloride, because i) their kinetic curve did not show a characteristic peak of an intermediate; ii) after the depletion of TCE, no decrease in the concentration of *cis*-DCE and vinyl chloride was found with prolonged reaction time. Rather, the acetylene should be formed directly from the reduction of TCE, without any steady-state intermediates.

Mass balance. We also noted that the carbon mass balance, which includes reactant and all the identified products in solution and gas phases, was approximately 70% at the end of reaction (at 90 min, Fig. 2**a**). To make clear the origination of this deficit, we heated the reacted suspension to 90 °C after stopping the reaction by dropping the pH to below 4.0, to thermally desorb the products potentially adsorbed on the surface of Co−NC. After that, the mass balance reached 98.7% (Fig. 2**c**), substantiating the deficit of the mass balance is due to the adsorption of the products on the Co−NC catalyst. The acetylene accounted for 83.3% of the products, which suggests that the sequestration of acetylene on the catalyst is stronger than that of other products. Taking into account ethene secondarily reduced from acetylene, the yield of acetylene should be nearly 90% (88.7%). Similarly, the results at pH 8.0 support all the conclusions made above, whilst more acetylene and ethene (92.9% in total) was produced (Fig. 2**c**), as discussed below.

pH effects. We further investigated the effect of pH on the Co−NC-catalyzed dechlorination of TCE and found the reaction was markedly enhanced at a higher pH. With the increasing pH from 5.0 to 9.0, the reaction rate constants increased exponentially from 0.26×10^{-3} to 0.28 min^{-1} (Fig. 2**d** and **S9**). This pH dependence was in agreement with the Ti(III)-citrate consumption during the reaction (Fig. S10). Moreover, pH also largely influenced the product distribution from TCE dechlorination. More acetylene and ethene were formed at higher pHs, and more than 94.8% of TCE was transformed to acetylene at pH 9.0 in 20 min, after taking the acetylene-derived ethene into account (Fig. 2**d**). This pH dependence could partly be attributed to the more negative reduction potential of the Ti(IV)/Ti(III) couple at higher pH (−60 mV per pH unit) [49]. However, this could not explain the pH dependence of product distribution, which is related to the dechlorination mechanism. One possible interpretation is lower proton concentration could further suppress the hydrodechlorination pathway, whilst consequently the acetylene pathway, in which no proton is involved in the rate-determining step, is enhanced relatively.

Cycling stability and impact of water matrix. The catalytic stability of the Co−NC was evaluated by a cycling test. Without any reactivation, the dechlorination rate of TCE did not decrease (Fig. 3**a**), nor did the product distribution change in five cycles (data not shown). During these five cycles, 0.50 mM TCE was consumed. The total amount of Co atoms in the used catalysts was 0.061 mM, implying that the turnover number of Co atoms was about 8 during this process. Moreover, the real turnover value should be greater than this value, because the surface-exposed Co sites should be less than the total Co atoms in the catalyst. The influence of co-existing substrates was tested. Except for humic acid (HA), common co-existing ions showed little impact on the dechlorination rates (Fig. 3**b** and **S11**). According to the present data and previous studies on HA effect [50,51], the negative effect of HA may be ascribed more to the block of Co−NC surface by its adsorption, but less to its competition for electrons, because the consumption of Ti(III) by HA was not observed. We also tested the reaction rate in real groundwater. The rate was lower than that without co-existing matters (Fig. 3**b**), which may be ascribed to the HA or the organics similar to HA in the real groundwater because it was from a near-surface aquifer. Despite the negative effect of these organics, the rate was still comparable with the efficient dechlorination processes reported so far, and the removal capacity and product distribution were not affected, suggesting its considerable tolerance for common water matrics. In addition, this negative effect could be mitigated by increasing the loading of reactive sites and the surface, according to the discussion above.

Column experiments. Moreover, we conducted a column experiment to access the effectiveness and longevity of Co−NC in a typical remediation scenario using permeable reactive barrier technologies. In that experiment, the simulated TCE-contaminated groundwater passed

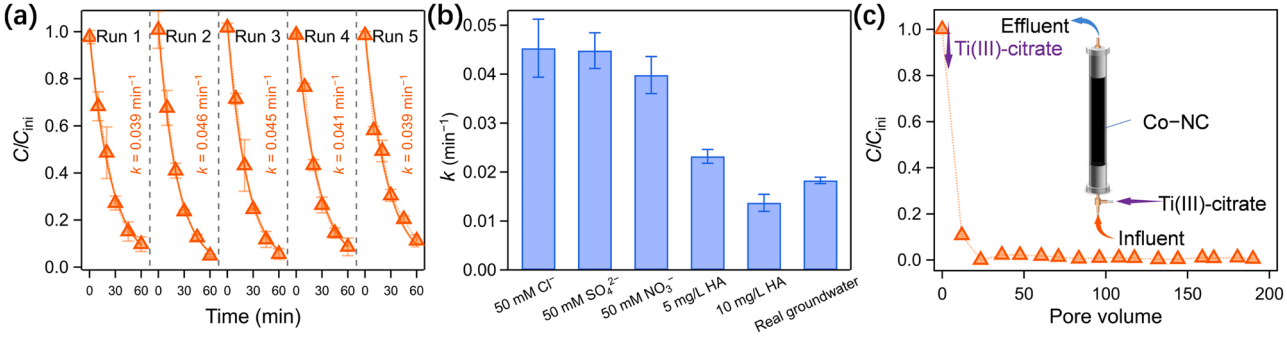

Fig. 3. (a) Kinetics of TCE dechlorination catalyzed by Co−NC in five cycles. Solid lines are the first-order fits. (b) The influence of common co-existing substrates and the water matrix of real groundwater on the first-order rate constants of TCE dechlorination. "HA" is the abbreviation for "humic acid". Reaction conditions of (a) and (b): $[TCE]_0$ = 0.1 mM, [Co−NC] = 0.2 g/L, $[Ti(III)]_0$ = 7.4 mM, pH was maintained at 7.0 with 50 mM HEPES buffer, T = 25 °C, anaerobic condition. (c) Residual TCE concentration in simulated groundwater pathed through a column bed packed with a mixture of Co−NC and sand. $[TCE]_0$ = 0.1 mM, 1.0 g Co−NC in the column, $[Ti(III)]_0$ = 5.0 mM, pH was 7.4, the experimental details and composition of the simulated groundwater can be found in the *Method* section in the Supplementary Material.

through the Co−NC-filled column and the residual TCE in the effluent was detected. As shown in Fig. 3**c**, the concentration of residual TCE is below 1% of the initial one, after the system was ready by adding Ti(III)-citrate to the influent and allowing for a period of time. The breakthrough of TCE did not take place within 200 pore volumes. These results indicate the excellent catalytic performance of Co−NC, which achieves rapid and complete dechlorination of TCE, and it exhibits superior stability for applications to the remediation of contaminated groundwater. Also, it should be noted that Co−NC used in this study was stored in the air, which did not cause any irreversible deactivation, showing much higher oxygen tolerance than RDases do.

3.3. Feasibility of employing Fe(II) as the electron donor

In pursuing a more feasible way to supply electrons for groundwater decontamination, we sought for a more engineeringly available electron donor. Among a series of inexpensive candidates, ferrous ion (Fe(II)) would be the most promising one considering its cost and environmental impact. As shown in Fig. 4**a**, TCE could be dechlorinated in the presence of dissolved Fe(II) and Co−NC. Except for the lower dechlorination rate, the Fe(II)/Co−NC system gave a similar product distribution to the Ti(III)-citrate system, with acetylene as dominant products. In contrast, little TCE was converted in the VB_{12} system with Fe(II) under identical conditions (Fig. S12). Although it was recently reported that TCE can be partially reduced by clay-activated Fe(II) in hundreds of days [52,53]. This study is the first to convert all the TCE in a practical time scale, 48 h, with dissloved Fe(II) as the electron donor. It shows the possibility to construct dechlorination systems with dissolved Fe(II), which could be more practical after the electron efficiency and kinetics issues are addressed in the future. We also detected the concentration of dissolved Fe(II) and confirmed solid ferrous (hydr)oxides were not responsible for this reaction. At a higher pH, Fe(II) will form solid precipitates and the rate will decrease, while below that pH (~9), the pH dependence of this system would be similar to that in Ti(III) systems. In addition, the kinetic curve in Fig. 4a does not show a transition from a fast to a slower reaction, but is consistent with simple first-order appearance kinetics, suggesting the Fe(III) generated during the reaction did not affect the catalytic activity of Co−NC. Also, the potential Fe precipitation in the filter reactors could be dissolved by simply washing it using diluted acid to recover the activity.

Fe(II) could be originated from the dissolution of ferrous minerals, which are one of the most earth-abundant and low-cost reductants. Additionally, the introduction of Fe(II) into the system could be energy-free by simply dosing or rainfall infiltration through soil to chlorinated ethenes-containing water. Actually, those processes are occurring naturally, leading to the ubiquitous Fe(II) in the aqueous environment, especially as an inherent soluble component in groundwater. Although it is a relatively weak reactant, its ability to donate electrons at neutral and alkaline conditions enables it to serve as the electron donor in the groundwater, the common pH of which falls into that working range. Therefore, utilizing Fe(II) as the electron donor is cost-efficient and does not require additional energy input and complex operation, making the Fe(II)/Co−NC system remarkably sustainable and techno-economically viable for groundwater remediation. Accordingly, we tested the performance of the Fe(II)/Co−NC system in real groundwater (Fig. 4**b**). About 70% of TCE was converted in 48 h, and at least 45% of it were transformed to acetylene, without taking into account the adsorbed acetylene.

3.4. Catalytic mechanisms

As mentioned above, VB_{12} with the Co−N_4 site lies at the heart of most RDases, and its reaction chemistry for the dechlorination of chlorinated ethenes has been extensively investigated [24]. Thus, the comparison between the VB_{12} and Co−NC systems can provide mechanistic insights into the catalytic pathway of Co−NC. Fig. 5**a** shows the kinetics and products of TCE dechlorination catalyzed by VB_{12}. For comparison, the same conditions and VB_{12} dosage (by Co content) as those for Co−NC experiments (Fig. 2**a**) were employed. At pH 7.0, the dechlorination rate constant of TCE (0.041 min^{-1}) on Co−NC was ~14 times higher than that in the presence of VB_{12} (0.29×10^{-2} min^{-1}). Moreover, the main product in the VB_{12}-catalyzed system was *cis*-DCE (93.0%), and little amount of other products such as acetylene was observed [54]. At pH 9.0, despite a slightly higher rate, the main product was still *cis*-DCE (Fig. S13) [54]. In comparison, acetylene was the main product at pH 5.0–9.0 in Co−NC systems, indicative of different reaction pathways between these two systems.

Furthermore, in the Co−NC system, we tested the dechlorination kinetics of PCE, which contains one more chlorine substituent than TCE. Accompanied by the rapid decrease of PCE, acetylene, and TCE were the dominant products. Remarkably, TCE was formed at the initial stage, but underwent a decay with the prolonged reaction time. Such a trend is a typical characteristic of a consecutive reaction, in which the initially formed TCE from PCE reduction can be further reduced to acetylene (PCE→TCE→acetylene). However, the kinetic fitting with the consecutive reaction as the only pathway did not well reproduce the evolution of both TCE and acetylene (Fig. S14), which suggests that the one-step complete dechlorination of PCE to acetylene (PCE→acetylene) is also

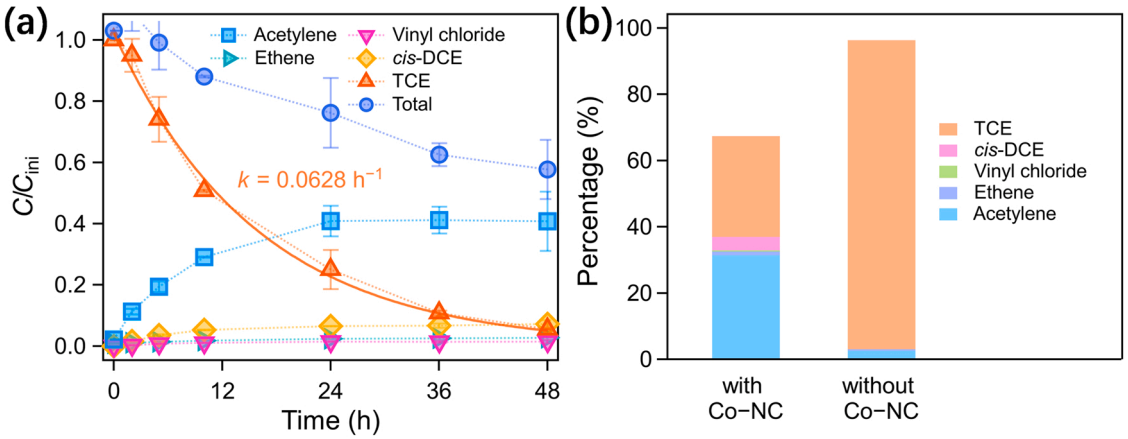

Fig. 4. (a) Kinetics of TCE dechlorination catalyzed by Co−NC (1.8 wt% Co) with Fe(II) as the electron donor. The solid line is the first-order fit. Reaction conditions: $[TCE]_0$ = 0.1 mM, [Co−NC] = 0.2 g/L, $[Fe(II)]_0$ = 10 mM, pH was maintained at 8.0 with 50 mM HEPES buffer, T = 25 °C, anaerobic condition. (b) Transformation of TCE in real groundwater in 48 h with Fe(II) as the electron donor. The data are the average values from duplicate experiments. Reaction conditions: $[TCE]_0$ = 0.03 mM, [Co−NC] = 0.2 g/L, $[Fe(II)]_0$ = 8 mM ($FeSO_4$), initial pH was 7.4 and not controlled during the reaction, T = 25 °C, anaerobic condition.

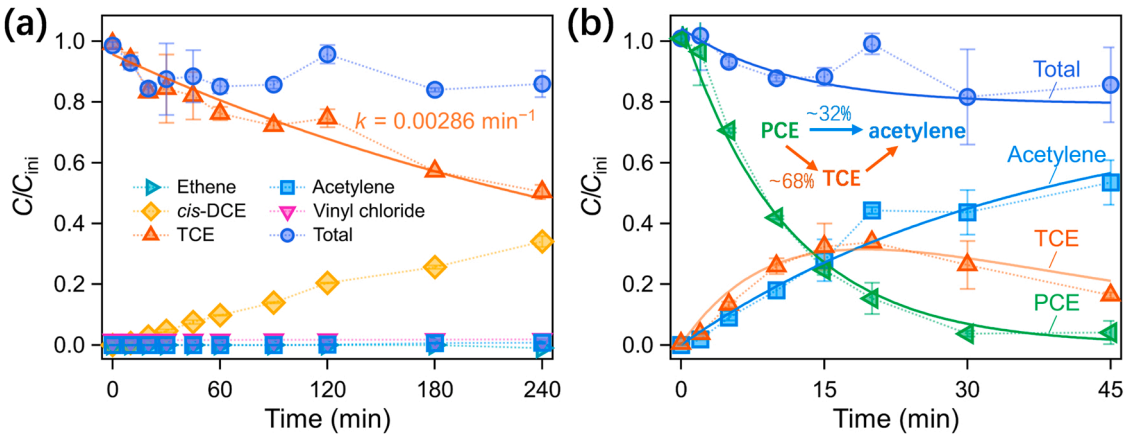

Fig. 5. (a) Kinetics of TCE dechlorination catalyzed by VB_{12} at pH 7.0. The solid line is the first-order fit. Reaction conditions: $[TCE]_0 = 0.1$ mM, $[VB_{12}] = 3.6$ mg Co L^{-1}, $[Ti(III)]_0 = 7.4$ mM, pH was maintained at 7.0 with 50 mM HEPES buffer, T = 25 °C, anaerobic condition. Solid lines are the first-order fits. (b) Kinetics of PCE transformation and the generation of its products. Solid lines are the fits using the derived model, which assumes that acetylene is generated from the dichotomous dechlorination of PCE parallelly and is elaborated in *Method* section in the Supplementary Material. Reaction conditions: $[PCE]_0 = 0.1$ mM, [Co−NC] = 0.2 g/L, $[Ti(III)]_0 = 7.4$ mM, pH was maintained at 7.0 with 50 mM HEPES buffer, T = 25 °C, anaerobic condition.

operative. Actually, the model by considering both the two pathways (elaborated in the Supplementary Material) fitted well with the data (Fig. 5**b**). The fitting results give a rate constant of 0.0213 min^{-1} for the one-step transformation of PCE to acetylene, and 0.0448 min^{-1} for the TCE-mediated pathway, which means that ~32% of PCE was transformed to acetylene via a one-step, multi-electron pathway. Due to its stronger electron-withdrawing effects of chlorine substituents, notably, PCE is more favorable to remove its first chlorine atoms via hydrodechlorination pathway to TCE, as discussed below. Nevertheless, these pathways can still avoid the formation of chlorinated intermediates.

Considering the same reactive site of VB_{12} and Co−NC but different product distribution resulted from them, the unique catalytic dechlorination behavior of the Co sites in Co−NC should be determined by the electronic interaction of Co sites with the NC support. To shed light on the role of NC support in the catalytic dechlorination, we performed cyclic voltammogram (CV) measurements on the catalysts loaded on an electrode with Nafion (Fig. 6**a**). Compared to the working electrode with only Nafion, a much larger reduction current was observed on the NC-loaded electrode during the negative scan, and a withdrawal of electrons from the electrode occurred on the reversal scan, which is typical behavior for capacitive-like charging/discharging of the NC materials [55,56]. The Co−NC showed a similar CV curve to that of NC material. Although Co is able to be converted to a lower chemical state suggested by semi-in situ XANES (Fig. S15), the CV curve of Co−NC did not show a notable peak of Co, probably due to its very low content (~0.44 atom %). In the presence of TCE, an obvious reduction current with an onset potential of ca. − 0.6 V vs. SHE appeared, which is much more positive than that of pure NC (ca. −1.5 V vs. SHE) and Nafion (ca. −1.8 vs. SHE, Fig. S16), indicating that the Co−NC has a high catalytic activity of reductive dechlorination.

The charging/discharging behavior endows the NC support with electron-storage ability, which may be essential to catalytic activity of Co−NC for the dechlorination. To verify this, we first added the Co−NC catalyst into 5 mM Ti(III)-citrate without TCE. By this way, the electron was pre-stored in the Co−NC, companying with the loss of Ti(III)-citrate (Fig. S17). When the concentration of Ti(III)-citrate decreased to 2.5 mM, TCE was injected. It turns out that the TCE decay rate ($k = 0.0372$ min^{-1}) was much higher than that initiated with 2.5 mM Ti(III)-citrate ($k = 0.0154$ min^{-1}) and even higher than that started with 5.0 mM Ti(III)-citrate ($k = 0.0310$ min^{-1}) (Fig. 6**b**). In another experiment, during the Co−NC-catalyzed TCE dechlorination, we suddenly dropped the pH from 7.0 to 4.0 to retard the electron-donating ability of Ti(III)-citrate. This pH drop did not stop the reaction immediately, and it continued for about 10 min (Fig. 6**c**). Given that negligible TCE reduction occurred at an initial pH below 5.0 (Fig. S9), this additional reaction at pH 4.0 should be driven by the electrons stored in the Co−NC at pH 7.0. All these observations indicate that the electron-storage ability of the NC support plays an important role in the catalytic dechlorination.

We further investigated the electronic structures of Co−NC using density functional theory (DFT) calculations, and compared it with the well-studied truncated 4-coordinated VB_{12} catalysis [37]. The calculating model of Co−N_4-embedded

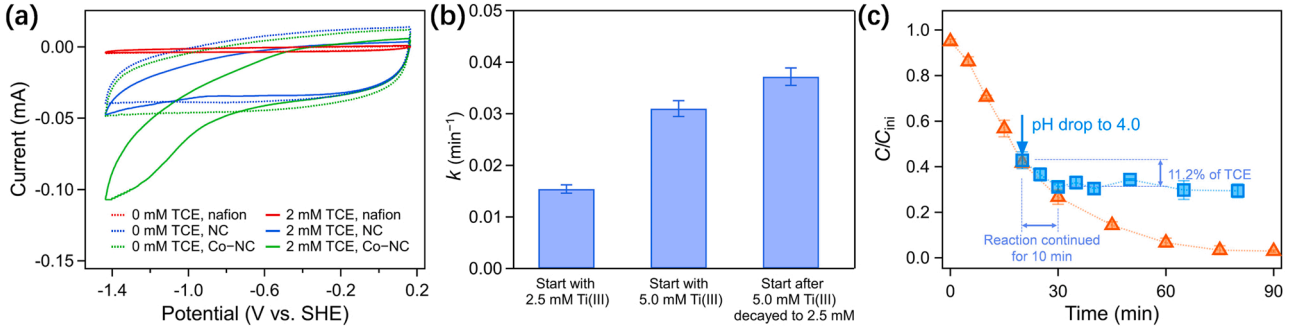

Fig. 6. (a) Cyclic voltammograms on Co−NC and NC working electrodes with or without TCE in acetonitrile. Scan rate: 100 mV/s. All the Co content in Co−NC in the related experiments is 1.8 wt%. (b) Dechlorination rate of TCE with Co−NC pre-equilibrated in 5.0 mM Ti(III)-citrate until it decayed to 2.5 mM, and the comparison with those start with 2.5 or 5.0 mM Ti(III). (c) Influence of pH sudden drop to 4.0 at 20 min on TCE decay. Reaction conditions of (b) and (c): $[TCE]_0 = 0.1$ mM, [Co−NC (1.8 wt% Co)] = 0.2 g/L, $[Ti(III)]_0 = 7.4$ mM, pH was maintained at 7.0 with 50 mM HEPES buffer, T = 25 °C, anaerobic condition.

graphene sheet and is shown in Fig. 7**a**. We first analyzed the frontier molecular orbitals of the Co−NC, which will be involved in the catalytic reactions. It is found that its HOMO is derived mainly from the Co 3d, together with minor π orbital of the NC structure, while the LUMOs (LUMO, LUMO+1, LUMO+2, and LUMO+3) are dominantly π-based, which are delocalized on the NC conjugated plane (Fig. S18). In addition, the energy gap between the LUMO and HOMO is only 0.1415 eV, and the energy distribution among the LUMOs is quite dense. In the actual Co−NC material, where the NC conjugated structure is extended on a much larger scale, state density just above the Co 3d-based state should be much higher. This unoccupied state can accommodate electrons from the electron donors and support the charge-storage ability of the Co−NC. Such an electronic structure of Co−NC material is important for its catalytic performance of dechlorination. Firstly, the main contribution of Co 3d to the HOMO suggests that the reduced Co center is first formed during the reduction of the Co−NC and it resembles the active state of cob(I)alamin (reduced VB_{12}), which can catalyze the efficient C−Cl cleavage. Secondly, the charge-storage ability of Co−NC enables it to store multiple electrons and they could be consecutively transferred to chlorinated intermediates that bind on the Co sites. Thus, the electrons become more available, which is favorable for the consecutive multiple-electron transfer during dechlorination. In contrast, for cob(I)alamin, the energy gap between the π-based LUMO and Co 3d-derived HOMO is rather large (1.2308 eV) [57], so that only the redox reaction of Co center is dominantly involved during the catalytic cycle, without electron-storage by the corrin ring, favoring the stepwise pathway.

Three mechanisms have been proposed for VB_{12}-catalyzed TCE dechlorination [24]: nucleophilic addition, electron transfer, and nucleophilic substitution. Among them, only nucleophilic substitution could lead to alkynyl-based products (acetylene). This mechanism starts from the nucleophilic attack by Co(I) of the cob(I)alamin, which cleaves the C−Cl bond and produces cobalamin vinyl complexes. The further reduction of this vinyl complex to its anion cleaves the Co−C bond and leads to DCE release in the VB_{12} system [24,58]. The nucleophilic substitution is proposed to be the dominant mechanism for Co−NC-catalyzed TCE dechlorination, due to the product distribution and its pH dependence mentioned above. Compare with the prior study on a Co-site biomimetic catalyst [33], a similar pathway for the first C−Cl bond cleavage is supposed, but its overall mechanism is stepwise hydrodechlorination, which may be ascribed to the chemical structure of the target contaminant (it has only α Cl atoms). In this study, the nucleophilic substitution in the Co−NC system formed a complex resembling the cobalamin vinyl complex by VB_{12}, while not easy to decompose as the latter does. To provide more insights into the different preferences for the formation of DCE and acetylene from the complexes by VB_{12} and Co−NC, we compared the LUMO of their dichlorovinyl complex, where the coming electron would populate for the formation of the complex anion. As shown in Fig. 7**b**, LUMO of dichlorovinyl-VB_{12} complex consists of the σ_{Co-C}* orbital, with a minor component of corrin macrocycle π * orbital, while Co−NC complex has LUMO associated with mixed π * and σ_{Co-C}* orbital. Accordingly, the C−Co fragment contributes to 68.1% of LUMO of dichlorovinyl-VB_{12} complex, while only 37.7% of LUMO of Co−NC complex is from that fragment. Such an LUMO character suggests that an electron during the formation of an anion mainly enters the σ_{Co-C}* antibonding orbital for the VB_{12} complex, which would weaken the Co−C bond. However, for the Co−NC complex, since most of the electron is distributed over the π * orbital, the weakening of Co−C should be much smaller than that of VB_{12} complex. To further confirm this proposal, we compared the change in the C−Co bond between the dichlorovinyl complex and its anion. The C−Co bond of dichlorovinyl-VB_{12} complex is elongated from 1.914 Å to 2.061 Å (Δ = 0.147 Å), while the increase in C−Co bond length of Co−NC complex is only 0.058 Å (from 1.903 Å to 1.961 Å) after the reduction of dichlorovinyl complex to its anion. Therefore, the C−Co bond in the Co−NC complex anion is quite difficult to cleave, which prevents the escape of DCE. Instead, it is more favorable that the dichlorovinyl complex anion undergoes further elimination reaction, and leads to the non-chlorinated acetylene products finally (Fig. 7**c**). Therefore, besides its excellent electron-storage ability, the electronic delocalization characteristic of the large π-conjugated structure of nitrogen-doped carbon support should be another key factor that enables the consecutive multiple-electron transfer pathway by Co−NC catalyst. Additionally, for the trichlorovinyl-Co−NC complex formed from PCE dechlorination, the contribution of σ_{Co-C}* antibonding orbital to its LUMO (47.1%) and the elongation of C−Co bonds after reducing to its anion (Δ = 0.091 Å) are much greater than those of dichlorovinyl one. The trichlorovinyl fragment is consequently easier to release from the complex anion, which can explain well the occurrence of hydrodechlorination and the formation of TCE.

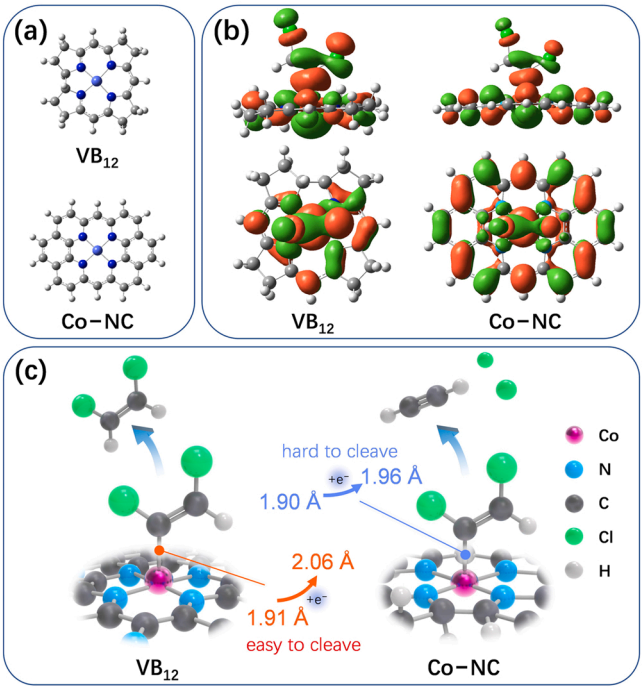

Fig. 7. (a) The models of Co−NC and VB_{12} used in DFT calculations. The calculating model of Co−NC was adapted from Co−N_4-embedded graphene sheet and the carbon atom along the edge was saturated by hydrogen. (b) Isosurface plots for the lowest unoccupied molecular orbitals (LUMOs) of dichlorovinyl-VB_{12} and dichlorovinyl-Co−NC complexes. (e) The effect of intermediate binding on the products distribution.

4. Conclusions

Combining the advantages of abiotic and biological dechlorination strategies may lead to a novel strategy that is robust enough under benign and easily scalable conditions. In this study, we embedded the enzyme-like Co−N_4 sites in the nitrogen-doped carbon support to fabricate the Co−NC catalyst and further construct a catalytic system for the full dechlorination of chlorinated ethenes. Up to 94.8% of TCE could be transformed to non-toxic acetylene and ethene in Co−NC systems. The Co−NC catalyst exhibited excellent stability for recycling and long-term performance even under the influence of co-existing substrates. These catalytic properties stem from the synergism of the catalytic activity of Co sites and the support effects of the nitrogen-doped carbon support. This synergism favors a mechanism where the toxic chlorinated intermediates are bound on Co sites until the full dechlorination, due to the excellent electron-storage ability and the electronic delocalization characteristic of nitrogen-doped carbons.

From the aspect of practical application, this system is compatible

with present groundwater remediation infrastructures, with the Co−NC serving as the filling material of permeable reactive barriers. Additionally, the feasibility of Co−NC to employ Fe(II) as the electron donor endows it with remarkable sustainability and practicality, especially with further investigation using Fe(II) at lower concentrations. These promising catalytic properties created by rational designing provide possibilities to develop new strategies. The Co−NC-based strategies are potentially much more sustainable than conventional dechlorination processes, because Fe(II) is the most common component in the groundwater. A possible corollary to these results is that an input-free remediation strategy for contaminated sites could be accordingly established based on Co−NC, or other catalysts, by utilizing the co-existing Fe(II) or other possible weak reductants in the environment in future studies.

CRediT authorship contribution statement

Hejie Qin: Conceptualization, Methodology, Formal analysis, Investigation, Resources, Data curation, Writing – original draft preparation, Visualization. **Tanjie Zha:** Investigation, Resources. **Kun Qian:** Investigation, Resources. **Yuankui Sun:** Writing – review & editing, Visualization. **Xiaohong Guan:** Data curation, Writing – review & editing, Supervision, Project administration, Funding acquisition. **Chuncheng Chen:** Conceptualization, Methodology, Validation, Formal analysis, Writing – review & editing.

Declaration of Competing Interest

The authors declare that they have no known competing financial interests or personal relationships that could have appeared to influence the work reported in this paper.

Data availability

Data will be made available on request.

Acknowledgements

This work was supported by the National Natural Science Foundation of China (Grant No. 22025601 and 22006114), and China Postdoctoral Science Foundation (2019M661628). Author Hejie Qin acknowledges supports from the Shanghai Super Postdoctoral Program. The author Hejie Qin thanks Wu Yuen's research group (University of Science and Technology of China) because he has learned a lot in that group.

Appendix A. Supporting information

Supplementary data associated with this article can be found in the online version at doi:10.1016/j.apcatb.2023.122459.

References

[1] J.M. Carter, W.W. Lapham, J.S. Zogorski, Occurrence of volatile organic compounds in aquifers of the United States, J. Am. Water Resour. 44 (2008) 399–416.
[2] L.-Z. Huang, Y. Wang, J. Deng, J. Yuan, Y. Dai, W. Yin, Generation of adsorbed atomic hydrogen by Pd(II) doped Fe(OH)2 enables ultra-fast reductive dechlorination of trichloroethylene, Appl. Catal. B Environ. 322 (2023), 122094.
[3] S.K. Chen, H.Y. Yang, S.R. Huang, J.M. Hung, C.J. Lu, M.H. Liu, Complete degradation of chlorinated ethenes and its intermediates through sequential anaerobic/aerobic biodegradation in simulated groundwater columns (complete degradation of chlorinated ethenes), Int. J. Environ. Sci. Technol. 17 (2020) 4517–4530.
[4] B. Heckel, S. Cretnik, S. Kliegman, O. Shouakar-Stash, K. McNeill, M. Elsner, Reductive outer-sphere single electron transfer is an exception rather than the rule in natural and engineered chlorinated ethene dehalogenation, Environ. Sci. Technol. 51 (2017) 9663–9673.
[5] S. Xiao, Z. Jin, H. Dong, J. Xiao, Y. Li, L. Li, R. Li, J. Chen, R. Tian, Q. Xie, A comparative study on the physicochemical properties, reactivity and long-term performance of sulfidized nanoscale zerovalent iron synthesized with different kinds of sulfur precursors and procedures in simulated groundwater, Water Res 212 (2022), 118097.
[6] F. Gao, H. Lyu, S. Ahmad, S. Xu, J. Tang, Enhanced reductive degradation of tetrabromobisphenol A by biochar supported sulfidated nanoscale zero-valent iron: Selectivity and core reactivity, Appl. Catal. B Environ. 324 (2023), 122246.
[7] S. Ailawar, A. Hunoor, B. Rudzinski, G. Celik, L. Burel, J.-M. Millet, J.T. Miller, P. L. Edmiston, U.S. Ozkan, On the dual role of the reactant during aqueous phase hydrodechlorination of trichloroethylene (HDC of TCE) using Pd supported on swellable organically modified silica (SOMS), Appl. Catal. B Environ. 291 (2021), 120060.
[8] Y. Xu, Z. Yao, Z. Mao, M. Shi, X. Zhang, F. Cheng, H. Yang, H. Tao, B. Liu, Single-Ni-atom catalyzes aqueous phase electrochemical reductive dechlorination reaction, Appl. Catal. B Environ. 277 (2020), 119057.
[9] M. Qiwen, K.H. Kim, I. Han, Correlation analysis of pollutant factors influencing the sulfite/UV-L advanced reduction process, KSCE J. Civ. Eng. 22 (2018) 475–481.
[10] B.-E. Jugder, H. Ertan, S. Bohl, M. Lee, C.P. Marquis, M. Manefield, Organohalide respiring bacteria and reductive dehalogenases: key tools in organohalide bioremediation, Front. Microbiol. 7 (2016) 249.
[11] Y.C. Kuo, S.H. Liang, S.Y. Wang, S.H. Chen, C.M. Kao, Application of emulsified substrate biobarrier to remediate TCE-contaminated groundwater: pilot-scale, Study, J. Hazard. Toxic. Radio. 18 (2014) 04014006.
[12] Z. Xiao, W. Jiang, D. Chen, Y. Xu, Bioremediation of typical chlorinated hydrocarbons by microbial reductive dechlorination and its key players: a review, Ecotoxicol. Environ. Saf. 202 (2020), 110925.
[13] E.J. Bylaska, A.J. Salter-Blanc, P.G. Tratnyek, One-electron reduction potentials from chemical structure theory calculations, in: S.B. Haderlein, T.J. Grundl, P. G. Tratnyek (Eds.), Aquatic redox chemistry, American Chemical Society, Washington, DC, 2011, pp. 37–64.
[14] M. Majone, R. Verdini, F. Aulenta, S. Rossetti, V. Tandoi, N. Kalogerakis, S. Agathos, S. Puig, G. Zanaroli, F. Fava, In situ groundwater and sediment bioremediation: barriers and perspectives at European contaminated sites, N. Biotechnol. 32 (2015) 133–146.
[15] D. Fan, D.M. O'Carroll, D.W. Elliott, Z. Xiong, P.G. Tratnyek, R.L. Johnson, A. Nunez, Garcia, Selectivity of nano zerovalent iron in, *situ* Chem. Reduct.: Chall. Improv., Remediat. 26 (2016) 27–40.
[16] A.N. Garcia, Y. Zhang, S. Ghoshal, F. He, D.M. O'Carroll, Recent advances in sulfidated zerovalent iron for contaminant transformation, Environ. Sci. Technol. 55 (2021) 8464–8483.
[17] B.P. Chaplin, M. Reinhard, W.F. Schneider, C. Schüth, J.R. Shapley, T. J. Strathmann, C.J. Werth, Critical review of Pd-based catalytic treatment of priority contaminants in water, Environ. Sci. Technol. 46 (2012) 3655–3670.
[18] V. Agarwal, Z.D. Miles, J.M. Winter, A.S. Eustáquio, A.A. El Gamal, B.S. Moore, Enzymatic halogenation and dehalogenation reactions: pervasive and mechanistically diverse, Chem. Rev. 117 (2017) 5619–5674.
[19] R. Shen, S. Zhang, Z. Liang, B. Mai, S. Wang, Mechanistic insight into co-metabolic dechlorination of hexachloro-1,3-butadiene in *Dehalococcoides*, Water Res 220 (2022), 118725.
[20] K.A.P. Payne, C.P. Quezada, K. Fisher, M.S. Dunstan, F.A. Collins, H. Sjuts, C. Levy, S. Hay, S.E.J. Rigby, D. Leys, Reductive dehalogenase structure suggests a mechanism for B12-dependent dehalogenation, Nature 517 (2015) 513–516.
[21] M. Bommer, C. Kunze, J. Fesseler, T. Schubert, G. Diekert, H. Dobbek, Structural basis for organohalide respiration, Science 346 (2014) 455–458.
[22] C. Kunze, M. Bommer, W.R. Hagen, M. Uksa, H. Dobbek, T. Schubert, G. Diekert, Cobamide-mediated enzymatic reductive dehalogenation via long-range electron transfer, Nat. Commun. 8 (2017) 15858.
[23] K. Thangavadivel, W.H. Wang, V. Birke, R. Naidu, A comparative study of trichloroethylene (TCE) degradation in contaminated groundwater (GW) and TCE-spiked deionised water using zero valent iron (ZVI) under various mass transport conditions, Water Air Soil Poll. 224 (2013) 1718.
[24] B. Heckel, K. McNeill, M. Elsner, Chlorinated ethene reactivity with vitamin B_{12} is governed by cobalamin chloroethylcarbanions as crossroads of competing pathways, ACS Catal. 8 (2018) 3054–3066.
[25] L. Jiao, H. Yan, Y. Wu, W. Gu, C. Zhu, D. Du, Y. Lin, When nanozymes meet single-atom catalysis, Angew. Chem. Int. Ed. 59 (2020) 2565–2576.
[26] Y. Peng, B. Lu, S. Chen, Carbon-supported single atom catalysts for electrochemical energy conversion and storage, Adv. Mater. 30 (2018) 1801995.
[27] H. Yan, C. Su, J. He, W. Chen, Single-atom catalysts and their applications in organic chemistry, J. Mater. Chem. A 6 (2018) 8793–8814.
[28] Y. Chen, S. Ji, C. Chen, Q. Peng, D. Wang, Y. Li, Single-atom catalysts: synthetic strategies and electrochemical applications, Joule 2 (2018) 1242–1264.
[29] K. Qian, H. Chen, W. Li, Z. Ao, Y.-n Wu, X. Guan, Single-atom Fe catalyst outperforms its homogeneous counterpart for activating peroxymonosulfate to achieve effective degradation of organic contaminants, Environ. Sci. Technol. 55 (2021) 7034–7043.
[30] C. Ren, P. Yang, J. Sun, E.Y. Bi, J. Gao, J. Palmer, M. Zhu, Y. Wu, J. Liu, A. Bioinspired, Molybdenum catalyst for aqueous perchlorate reduction, J. Am. Chem. Soc. 143 (2021) 7891–7896.
[31] C. Ren, E.Y. Bi, J. Gao, J. Liu, Molybdenum-catalyzed perchlorate reduction: robustness, challenges, and solutions, ACS EST Eng. 2 (2022) 181–188.
[32] Y. Li, S.L. Zhang, W. Cheng, Y. Chen, D. Luan, S. Gao, X.W. Lou, Loading single-Ni atoms on assembled hollow N-rich carbon plates for efficient CO_2 electroreduction, Adv. Mater. 34 (2022) 2105204.
[33] Y. Min, X. Zhou, J.-J. Chen, W. Chen, F. Zhou, Z. Wang, J. Yang, C. Xiong, Y. Wang, F. Li, H.-Q. Yu, Y. Wu, Integrating single-cobalt-site and electric field of boron nitride in dechlorination electrocatalysts by bioinspired design, Nat. Commun. 12 (2021) 303.

[34] S. Kabir, K. Artyushkova, A. Serov, B. Kiefer, P. Atanassov, Binding energy shifts for nitrogen-containing graphene-based electrocatalysts–experiments and DFT calculations, Surf. Interface Anal. 48 (2016) 293–300.
[35] I. Dror, M.A. Schlautman, Role of metalloporphyrin core metals in the mediated reductive dechlorination of tetrachloroethylene, Environ. Toxicol. Chem. 22 (2003) 525–533.
[36] A. Parthasarathy, T.A. Stich, S.T. Lohner, A. Lesnefsky, R.D. Britt, A.M. Spormann, Biochemical and EPR-spectroscopic investigation into heterologously expressed vinyl chloride reductive dehalogenase (VcrA) from *Dehalococcoides mccartyi* Strain VS, J. Am. Chem. Soc. 137 (2015) 3525–3532.
[37] L. Ji, C. Wang, S. Ji, K.P. Kepp, P. Paneth, Mechanism of cobalamin-mediated reductive dehalogenation of chloroethylenes, ACS Catal. 7 (2017) 5294–5307.
[38] S.H. Vosko, L. Wilk, M. Nusair, Accurate spin-dependent electron liquid correlation energies for local spin density calculations: a critical analysis, Can. J. Phys. 58 (1980) 1200–1211.
[39] J.P. Perdew, K. Burke, M. Ernzerhof, Generalized gradient approximation made simple, Phys. Rev. Lett. 77 (1996) 3865.
[40] A. Schäfer, C. Huber, R. Ahlrichs, Fully optimized contracted Gaussian basis sets of triple zeta valence quality for atoms Li to Kr, J. Chem. Phys. 100 (1994) 5829–5835.
[41] W.J. Hehre, R. Ditchfield, J.A. Pople, Self-consistent molecular orbital methods. XII. further extensions of Gaussian-type basis sets for use in molecular orbital studies of organic molecules, J. Chem. Phys. 56 (1972) 2257–2261.
[42] M.J. Frisch, G.W. Trucks, H.B. Schlegel, G.E. Scuseria, M.A. Robb, J.R. Cheeseman, G. Scalmani, V. Barone, B. Mennucci, G.A. Petersson, H. Nakatsuji, M. Caricato, X. Li, H.P. Hratchian, A.F. Izmaylov, J. Bloino, G. Zheng, J.L. Sonnenberg, M. Hada, M. Ehara, K. Toyota, R. Fukuda, J. Hasegawa, M. Ishida, T. Nakajima, Y. Honda, O. Kitao, H. Nakai, T. Vreven, J.A. Montgomery Jr., J.E. Peralta, F. Ogliaro, M. Bearpark, J.J. Heyd, E. Brothers, K.N. Kudin, V.N. Staroverov, T. Keith, R. Kobayashi, J. Normand, K. Raghavachari, A. Rendell, J.C. Burant, S.S. Iyengar, J. Tomasi, M. Cossi, N. Rega, J.M. Millam, M. Klene, J.E. Knox, J.B. Cross, V. Bakken, C. Adamo, J. Jaramillo, R. Gomperts, R.E. Stratmann, O. Yazyev, A. J. Austin, R. Cammi, C. Pomelli, J.W. Ochterski, R.L. Martin, K. Morokuma, V. G. Zakrzewski, G.A. Voth, P. Salvador, J.J. Dannenberg, S. Dapprich, A.D. Daniels, O. Farkas, J.B. Foresman, J.V. Ortiz, J. Cioslowski, D.J. Fox, Gaussian 09, Revision D. 01 (http://www.gaussian.com), Gaussian, Inc.,, Wallingford CT, 2009.
[43] T. Lu, F. Chen, Multiwfn: a multifunctional wavefunction analyzer, J. Comput. Chem. 33 (2012) 580–592.
[44] Z. Yang, Y. Wang, M. Zhu, Z. Li, W. Chen, W. Wei, T. Yuan, Y. Qu, Q. Xu, C. Zhao, X. Wang, P. Li, Y. Li, Y. Wu, Y. Li, Boosting oxygen reduction catalysis with Fe–N_4 sites decorated porous carbons toward fuel cells, ACS Catal. 9 (2019) 2158–2163.
[45] A. Serov, K. Artyushkova, P. Atanassov, Fe−N−C oxygen reduction fuel cell catalyst derived from carbendazim: synthesis, structure, and reactivity, Adv. Energy Mater. 4 (2014) 1301735.
[46] M. Chen, N. Wang, L. Zhu, Single-atom dispersed Co−N−C: a novel adsorption−catalysis bifunctional material for rapid removing bisphenol A, Catal. Today 348 (2020) 187–193.
[47] Z. Wang, Y. Wang, W. Wang, D. Wu, Q. Wu, H. Hu, Highly selective production of singlet oxygen by manipulating the spin state of single-atom Co–N moieties and electron localization, Appl. Catal. B Environ. 324 (2023), 122248.
[48] W. Xie, S. Yuan, X. Mao, W. Hu, P. Liao, M. Tong, A.N. Alshawabkeh, Electrocatalytic activity of Pd-loaded Ti/TiO_2 nanotubes cathode for TCE reduction in groundwater, Water Res 47 (2013) 3573–3582.
[49] C. Holliger, A.J. Pierik, E.J. Reijerse, W.R. Hagen, A spectroelectrochemical study of factor F430 nickel(II/I,) methanogenic Bact. aqueous Solut., J. Am. Chem. Soc. 115 (1993) 5651–5656.
[50] H. Qin, D. Yin, J.Z. Bandstra, Y. Sun, G. Cao, X. Guan, Ferrous ion mitigates the negative effects of humic acid on removal of 4-nitrophenol by zerovalent iron, J. Hazard. Mater. 383 (2020), 121218.
[51] P.G. Tratnyek, M.M. Scherer, B. Deng, S. Hu, Effects of natural organic matter, anthropogenic surfactants, and model quinones on the reduction of contaminants by zero-valent iron, Water Res 35 (2001) 4435–4443.
[52] J. Entwistle, D.E. Latta, M.M. Scherer, A. Neumann, Abiotic degradation of chlorinated solvents by clay minerals and Fe(II): evidence for reactive mineral intermediates, Environ. Sci. Technol. 53 (2019) 14308–14318.
[53] J. Huang, A. Jones, T.D. Waite, Y. Chen, X. Huang, K.M. Rosso, A. Kappler, M. Mansor, P.G. Tratnyek, H. Zhang, Fe(II) redox chemistry in the environment, Chem. Rev. 121 (2021) 8161–8233.
[54] G. Glod, W. Angst, C. Holliger, R.P. Schwarzenbach, Corrinoid-mediated reduction of tetrachloroethene, trichloroethene, and trichlorofluoroethene in homogeneous aqueous solution: reaction kinetics and reaction mechanisms, Environ. Sci. Technol. 31 (1997) 253–260.
[55] K. Wan, Z.-p Yu, X.-h Li, M.-y Liu, G. Yang, J.-h Piao, Z.-x Liang, pH effect on electrochemistry of nitrogen-doped carbon catalyst for oxygen reduction reaction, ACS Catal. 5 (2015) 4325–4332.
[56] T. Lin, I.W. Chen, F. Liu, C. Yang, H. Bi, F. Xu, F. Huang, Nitrogen-doped mesoporous carbon of extraordinary capacitance for electrochemical energy storage, Science 350 (2015) 1508–1513.
[57] M.D. Liptak, T.C. Brunold, Spectroscopic and computational studies of Co^{1+}Cobalamin: spectral and electronic properties of the “superreduced” B_{12} cofactor, J. Am. Chem. Soc. 128 (2006) 9144–9156.
[58] K.M. McCauley, D.A. Pratt, S.R. Wilson, J. Shey, T.J. Burkey, W.A. van der Donk, Properties and reactivity of chlorovinylcobalamin and vinylcobalamin and their implications for vitamin B_{12}-catalyzed reductive dechlorination of chlorinated alkenes, J. Am. Chem. Soc. 127 (2005) 1126–1136.